Initial Condition Monitoring Experience on a Wind Turbine

Eric Bechhoefer[1], Mathew Wadham-Gagnon[2], and Bruno Boucher[3]

[1]*NRG Systems, Hinesburg, VT,05461,USA*
erb@NRGSystems.com

[2,3]*TechnoCentre éolien, Gaspé, Qc, G4X 1G2,Canada*
mgagnon@eolien.qc.ca
bboucher@eolien.qc.ca

ABSTRACT

The initial installation of a condition monitoring system (CMS) on a utility scale wind turbine produced a number of unexpected results. The CMS was installed on the TechnoCentre éolien Repower MM92. The installation allowed testing of a MEMS (microelecctromechanical system) based sensor technology and allowed and in-depth analysis of vibration data and revolutions per minute (RPM) data. A large 3/revolution effect, due to tower shadow and wind shear, required the development of an enhanced time synchronous average algorithm. The ability to easily measured changes in main rotor RPM, as a result of tower shadow and wind shear phenomenology, may also facilitate the detection of icing or blade pitch error.

1. INTRODUCTION

NRG System in collaborative partnership with TechnoCentre éolien, installed a CMS on a 2.05 MW Repower MM92 at the TechnoCentre's northern wind energy research location in Rivière-au-Renard. CMS allows operations and maintenance professionals to dramatically lower their costs by accurately predicting when components in the turbine's drive train are likely to fail months in advance. Maintenance and crane calls can then be scheduled at the most optimal time, such as during the low-wind season.

The goal of this collaboration is to validate the performance of a new CMS architecture and gain experience of CMS on a wind turbine. During the validation processes, both raw and processed data is available to NRG System and the TechnoCenter. The CMS installation consisted of:

- A two axis, low speed (1000 mv/g) MEMS accelerometer, used for measuring nacelle motion,
- Seven, High Speed (50 mv/g, 0-32 KHz) MEMS accelerometers for drivetrain monitoring,
- One tachometer (smart sensor), and
- A local data concentrator, which provides sensor control, temporary data storage, and Ethernet access.

The CMS was installed on a Repower MM92. This wind turbine uses a three stage, planetary gearbox with a total shaft rate increase of approximately 1:96. Power is generated from a double feed induction machine, allows the main shaft input rates to vary from 7 to 15 revolutions per minute (RPM, or 0.11 to 0.25 Hz). The CMS was configured to perform an acquisition every 10 minutes, and down load raw vibration data every 6 hours.

Most industrial accelerometers have an operational range from 2 Hz to 10 KHz. The rates and frequencies associated with many of the gearbox components are below this rate. In order to do analysis on these components, the CMS used MEMS based accelerometers instead of traditional lead zirconate titanate (PZT) based accelerometers. The CMS's MEMS devices have a response to DC, which makes them appropriate for this application.

It was important to validate this CMS on an operational wind turbine in that may many of the technologies have never before been implement in a CMS. For example, the CMS, in addition to validating MEMS accelerometers performance:

- Tested new packaging design using conductive plastics to lower packaging cost of the sensor (approximately 1/7 cost of stainless steel packages),
- Implemented all of the condition indicator (CI) processing and analysis (such as the time synchronous average, gear analysis (residual, energy operator, narrowband/amplitude

modulation/frequency modulation) and bearing envelope analysis) on the sensors themselves.

- Implemented a smart tachometer sensor which passed zero crossing data to all of the vibration sensors so that they can perform the shaft, gear and bearing analysis
- A bused sensor system to reduce the weight and cost of harnessing, and
- A cloud based user display, again to lower the setup and maintenance cost to the user.
- A true prognostic capability by providing an estimate of the remaining useful life of a component based on a physics of failure model.

Ultimately, it is anticipated that such architectures will deliver world class diagnostics/prognostic performance at a fraction of the cost of traditional, "star" architecture CMS using PZT accelerometers.

1.1. System Considerations with Using MEMS

The newest generation of MEMS accelerometers offers performance that in many cases is superior to traditional PZT devices *if it is packaged correctly*. MEMS accelerometers sense changes in capacitance, based on distance from a reference, instead of charge (piezoelectric effect) due to shear. Because of this physically different way to measure acceleration, these devices can measure from DC to 32 KHz. However, since MEMS accelerometers are capacitive sensor (vibration changes sensor capacitance, which is proportional to voltage), they are sensitive to electromagnetic interference (PZT have better electromagnetic noise immunity). As such, to ensure performance near a large generator, they must be packaged with an analog to digital converter at the sensor.

One disadvantage of MEMS accelerometers is that they are noisier than PZT accelerometers. The power spectral density of a typical accelerometer at 1 KHz is 10 to 190μg/√Hz (see Analog). Compare this to a wideband MEMS device, such as Analog Devices ADXL001 with 4mg/√Hz, or approximately 2 to 40 times noisier. That said, from a system perspective the data acquisition, processing and condition indicator (CI) generation gives significant process gain and a large reduction in noise.

As an example, a typical shaft analysis would result in a time synchronous average (TSA, Randal 2011, McFadden 1994) of length 8196 for 20 revolutions. The reduction in non-synchronous noise (part of which is accelerometer self noise) is the product of the process gain due to the TSA (1/√rev or 0.2236) and the noise reduction of the spectrum of the TSA (1/√(length/2) or 0.011), which in total is 0.0025 * the spectral density. This reduction is more than adequate for most CMS analysis. It was observed that use of a MEMS accelerometer does not significantly degrade the ability to detect component fault given the process gain of the CMS analysis.

1.2. Opportunities for Using MEMS

The MEMS accelerometer was packaged with the analog-to-digital converter (ADC) because it is sensitive to electromagnetic interference. This necessitates RAM to store the vibration data during the acquisition, a microcontroller to drive the ADC, and a receiver/transmitter to move data. By selecting a microcontroller with a floating point unit, it was possible to perform all of the processing of the vibration data on the sensor.

The sensor, when finished processing (about 20 seconds) sends condition indicator data to the local data concentrator. This greatly reduced to the overall system cost of the system by allowing the use of low cost microcontrollers vs. higher cost Intel or ARM based processors.

1.3. Tachometer Function

Because vibration processing is done locally at the sensor, the sensor will need zero crossing data to perform analysis on the components that it monitors. The zero crossing data is used for calculation of the time synchronous average.

A tachometer sensor was developed that, instead of sending the digitized output of the Hall Effect speed sensor, measured the zero crossing times (ZCT). The ZCT was then broadcast by the tachometer sensor to all vibration sensors on the network. The output of the Hall Effect speed sensor was tied to the microcontroller general purpose input/oupt (GPIO) pin. When the GPIO pin went high, the microcontroller measured the time from the last interrupt. The clock on the microcontroller was 100 MHz, with a jitter 20 parts per million.

2. INITIAL VETTING AND VERIFICATION

Following the installation in early December 2011, the CMS was evaluated to ensure:

- That the system MEMS based sensors were measuring vibration data,
- That the configuration was correct, and processing appropriate for Shaft, Gear and Bearing condition indicators.

The CMS was configured to acquire data for 40 seconds. As noted, the generator is a variable speed system: a lower limit of 11,000 rpm was set on the CMS to ensure that the CI collected would be taken at similar torque/rpm values. This gave a range of 7 to 12 revolutions on main rotor. At the high speed side (total gearbox ratio of 1:96) the output shaft and generator has 105 to 150 revolutions.

2.1. MEMS Accelerometer Accuracy

There was an initial concern that the MEMS accelerometer would be too noisy to accurately measure the vibration on the gearbox. Shaker table testing found that the MEMS accelerometers where typically within 2% error. This testing was conducted at higher frequencies and G values (needed because of the feedback system on the shaker itself) than would be seen on the planetary section of the wind turbine.

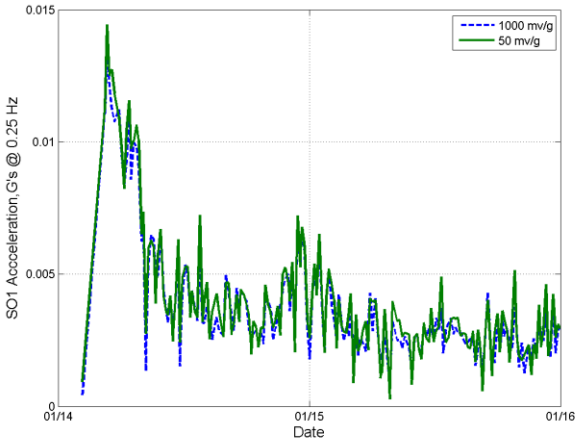

Figure 1 Comparison of Co-Located Sensor (1000 mv/g vs. 50 mv/g)

Two sensors where co-located on the main bearing of the turbine. The first sensor was a low frequency (0-20 Hz) sensor, 1000 mv/g, sampled at 1KHz. The second sensor was a high frequency (0-32 KHz) sensor, 50.4 mv/g, sampled at 3.3 Hz. This gives a time synchronous average (TSA) length of 32768 points. Over the course of the winter, a large SO1 values was measured on both sensors (and on the planetary carrier sensor as well). It was suspected that this was an icing event, which was subsequently confirmed (Figure 2). Because this was real signal, the SO1 between the two sensors should be seen and were compared to see how the high frequency (low gain) sensor performed relative to the more accurate, low frequency sensor (Figure 1).

The SO1 values were calculated from TSA with only 7 revolutions, at a shaft rate of .25 Hz. The correlation between the two sensors was 0.98, with a 4% bias error in the high frequency sensor. The RMS error is 5e-4 Gs. This is remarkable performance in detecting low G signals at low frequency. More so in that the high speed sensor is operating at only 0.007% of full range. This suggests that the MEMS accelerometers are capable of detecting gear faults in the planetary section of the gearbox.

Figure 2 Icing on Wind Turbine Blade

2.2. Tachometer and Main Rotor Speed Variation

It was immediately noted that the main rotor had large variations in speed over the 40 second acquisition. Because of the extremely low shaft rate (0.18 to .25 Hz), the acquisition must be extended long enough to capture an imbalance on the main rotor. Additionally, an acquisition on the Ring/Carrier/Planets must be long enough to generate valid TSA (admittedly, 7 revolutions is not a large number of revolutions). Because of the large variance in wind speed, it was found that variation in main rotor RPM average 0.5%. Some acquisitions had variations in RPM of greater than 2.5% (Figure 3).

These large variations in shaft speeds will be propagated throughout the gearbox, with the effect being greatest on the low speed shafts/gears. This is because the higher speed shafts require smaller acquisition times. As noted, the high speed shaft, which is turning 95.9 times faster than the low speed shaft, requires significantly less time to get one revolution. In fact, a six second acquisition results in 150 revolutions of the shaft.

Without some method to normalize the variation in shaft rate, there will be smearing in the spectrum (Figure 4). This example is taken from the planetary carrier sensor, where the 123 tooth ring gear frequency is clearly present at 27.2 Hz. There are three planets, and which will result in sidebands at 26.53 and 27.86 Hz (+/-3 * shaft rate, which for this acquisition was 0.22 Hz). In the Figure 4 subplots, the spectral representation of the raw spectrum is smeared. At higher harmonics (2^{nd} harmonic at 54.4 Hz, and 3^{rd} harmonic at 81.6Hz), the raw spectrum is hardly greater than the base noise.

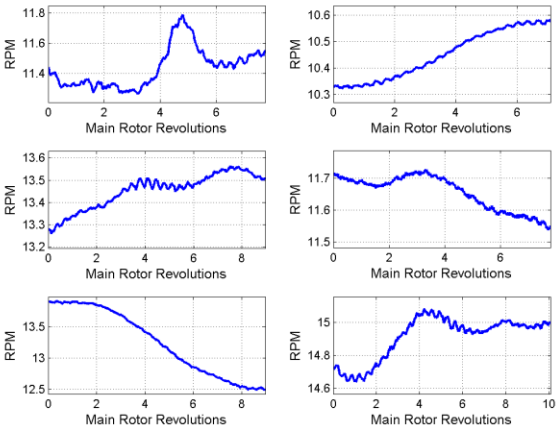

Figure 3 Examples of Main Rotor Speed Variations

This is in comparison to the TSA spectrum, which clearly shows the expected sidebands. Since many gear fault algorithms are based on the ratio of the gear mesh frequency to its sideband, without normalization, the ability to detect gear fault on the lower speed shaft is greatly reduced.

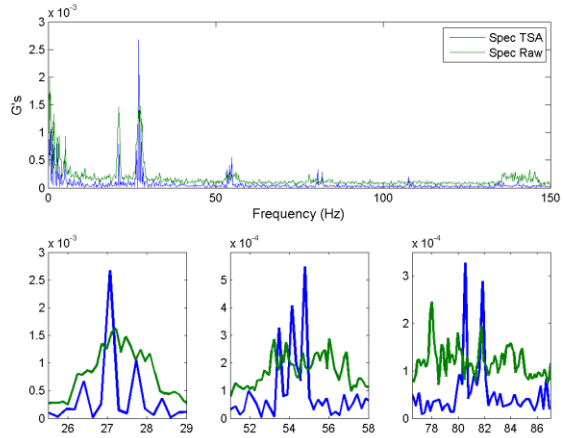

Figure 4 Comparison of Spectrum of TSA vs. Spectrum of Raw Vibration Data

2.3. The Need for Improved an TSA

The observant reader will note that in Figure 3, there is a ripple in the rotor speed. On closer observation (Figure 5), it is seen that there is a 3/revolution change in RPM overlaid on the RPM change as a result of changes in wind speed.

This phenomenology has been observed (Dolan, 2006) by wind turbine controls and power conversion engineers. These 3/rev oscillations are important from their perspective since they could have wide ranging effects on control systems and power quality. In systems connected directly to the grid, these torque oscillations could affect of grid power quality. For systems interfaced to the grid through converters, these torque oscillations would be more important in terms of converter control.

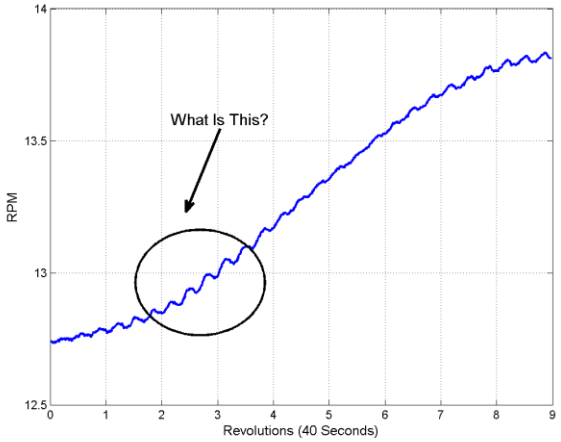

Figure 5 Example 3/Rev Torque Ripple

This torque ripple is the result of tower shadow and wind shear. Tower shadow occurs because the wind flow directly in front of the tower is stalled. As the blade passes in front of the tower at the bottom of the arc, it generates less lift which reduces the torque on the hub. Wind shear occurs because air is a viscous fluid: wind speed increases with height. As the blade reaches the top of the rotor arch, the blade generates more lift which increases the torque on the hub.

From a condition monitoring perspective, there has been no reporting of this shaft behavior. This could have deleterious effects on the performance of the TSA. Typically (McFadden (1997), Bechhoefer (2009)) the model for the TSA assumes linear increase/decrease in rotor speed. TSA using Spline interpolation could control a 1/rev torque ripple. The 3/rev torque ripple violates both methodologies. This required the development of an "enhanced" TSA algorithm.

Current TSA algorithms uses a tachometer input to calculate the time (and number of sampled data points) in one revolution of the shaft under analysis. The sampled data points are then re-sampled using linear/spline interpolation. In the enhanced TSA algorithm, each revolution was partitioned into 16 inter revolution sections, on which the data points were re-sampled (Figure 6).

16 inter revolution sections where used because:

- From Nyquist, to reconstruct the 3/rev, at least 6 sub-sections would be needed.
- The Fourier Transform used in this implementation was a Radix-2, thus the TSA always is a power of 2. To divide evenly, the sub-sections should also be a power of 2

- Both 8 and 16 inter revolution sections methods were tested, the 16 inter revolution section version had marginally improved performance (RMS error between re-sampled and original data).

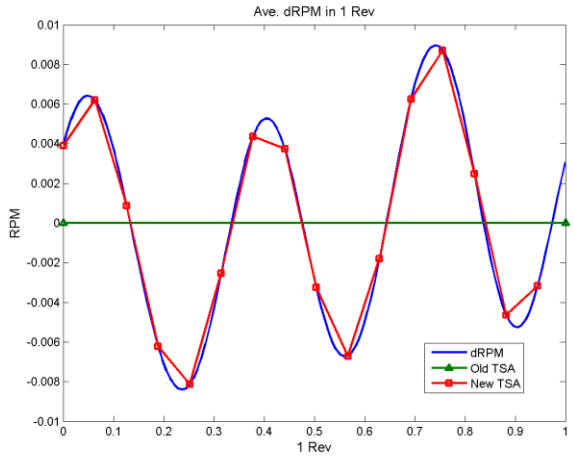

Figure 6 Comparison of the 3/Rev change in RPM, vs the TSA and "Enhanced" TSA

For example, the TSA for the carrier sensor, based on a .22 Hz shaft rate and a sample rate of 3296 sps, had 32768 data points. For each of the 16 inter revolution sections, the sampled vibration data was linear interpolated into 2048 data values.

In Figure 6, the TSA of the shaft RPM data was taken, and the result was de-trended. This represents the change in main rotor RPM over one revolution. The old/current TSA algorithm would resample the data linearly between one revolution. The enhanced TSA represents the 3/Rev change in RPM by "chopping" one revolution into 16 pieces, and linearly interpolating.

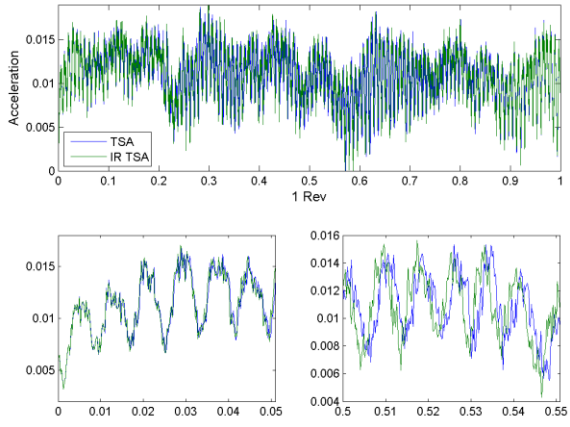

Figure 7. Difference in Phase Between Old and Enhanced TSA

The enhanced TSA better represents the phase changes of the vibration signal better than the original TSA (Figure 7).

In Figure 7, the two TSA algorithms start and end in phase (see subplot 1). However, the difference in phase soon becomes apparent. This phase error is similar to jitter, which reduces the ability of the FFT to produce an accurate spectrum. Similar to the comparison of a raw spectrum with a TSA spectrum, the enhanced TSA will show a better representation of the gearbox spectrum (Figure 8).

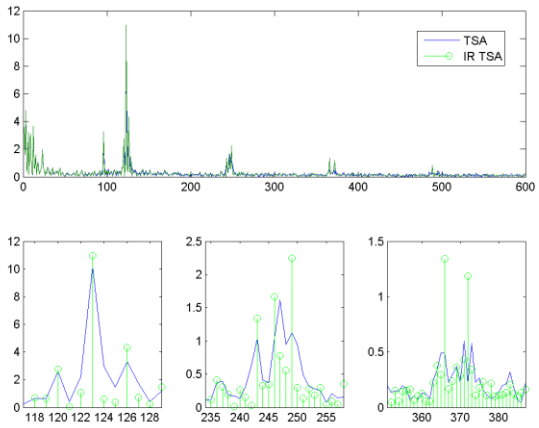

Figure 8 Difference in Spectrum Between Old and Enhanced TSA

Note that the enhanced TSA has more distinct side bands, and that the 2nd and 3rd harmonics of the ring gear are clearly more prominent that in the old/current TSA algorithm. The enhanced TSA algorithm itself did not greatly add to the processing time.

2.4. Inline Decimation in the TSA

There are two contending system issues when selecting the accelerometer sample rate. For bearing analysis, one needs to sample at a high enough sample rate to capture the structural resonance of the bearing. This is needed for bearing envelope analysis. For the TSA, one needs to sample at a low enough rate such that the length of the TSA is less than the maximum allowable FFT length (which is 32768 data points).

This becomes a problem for larger wind turbines (2MW and greater) where the main shaft rate is a faction of a Hertz. For example, consider main shaft with turning at 11 RPM (0.18 Hertz). For the main and carrier bearing, one would like capture the 2 KHz to 2.2 KHz window for bearing analysis. This requires sampling at greater than 4.4 KHz. The closest sample rate for the CMS is 6104 sps. For this shaft rate, the length of the TSA is:

(1)

This is longer the maximum allowable FFT. The next lower sample rate is 3052, but this is too low for the bearing analysis.

Because there is limited processing resources on the sensor, an inline low pass filter and decimate capability was added to the TSA:

- If the length of the TSA, n > 32768, then
  - Decimate = n/32768,
  - Filter coefficients are derived for a 4 point, FIR filter design, where the normalized frequency is 1/Decimate.
  - For Decimation of 2, b = [0.204 0.593 0.204]

The flow of the enhanced TSA algorithm is:

```
for 1 to # of TSA Revolution
   for 1 to 16 (the number of sub sections to capture 3/rev
   interpolate the vector of zero cross times
   get the change in time between the re-sampled data, dt.
    for the length of each sub section
      if decimate = 1 (no decimation)
         interpolate the data point at
            index, index + 1, for time dt.
      Else
          Interpolate the data point by filtering
            the data point at index -1,0,1 using b
            the data point at index 0,1,2 using b
```

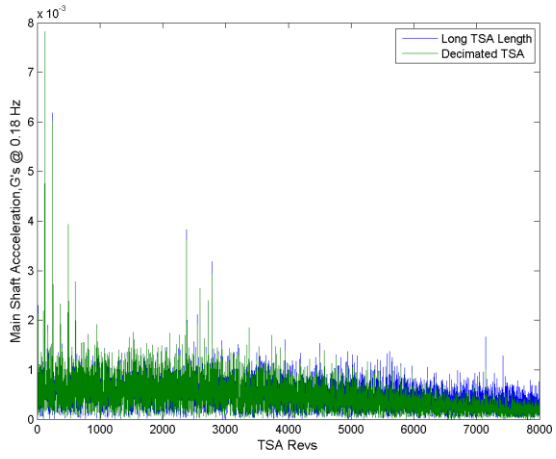

Figure 9 Effect on In-line Decimation on TSA Spectrum

This inline process allows the higher sample rate required for bearing analysis, and does not greatly increase the order of operations for the TSA algorithm. It does not affect the gear or shaft analysis at all. Shaft analyses measures the 1st, 2nd and 3rd harmonics (bin 2, 3 and 4 of the TSA FFT), while the gear diagnostics, which analysis higher harmonics, is improved. This is because of the reduction in higher frequency noise (Figure 9).

The ring gear is 123 teeth, giving the first 5 harmonics (up to bin 615). There are additional tones at 2382 through 2782 (which represent 428 to 500 hz values) are undetermined. Above this frequency, the spectrum is measuring broadband noise.

3. Validation of Bearing Fault Detection with MEMS Accelerometers

There is a concern that the high spectral noise floor of MEMS based accelerometers will make them an inappropriate sensor for bearing analysis. Early stage (stage 3) bearing faults have spectral content typically 3 orders or magnitude smaller than spectral content of gears or shafts. This makes fault detection difficult with even the lowest noise PZT accelerometers. To verify the ability to detect bearing faults, a test rig was developed on which nominal and faulted bearing could be run.

Both inner and outer races faults were developed. Testing was conducted with a shaft rate of 25 Hz, which is approximately the rate of wind turbine high speed shaft. The load on the bearing was varied from 0, 25, 50, 100, 150, 200, 250 and 300 lbs of load (the design load of the bearing was 1025 lbs.). Figure 10 is an example of the outer race fault.

Figure 10. Example Outer Race Fault

The outer race bearing fault rate was 80.4 Hz. Envelope analysis performed on the sensor was with windows of: 0.5-1.5 KHz, 2.5-3.5 KHz, 4-5 KHz, 9-10 KHz, 10-11 KHz, 13-14 KHz, and 22-24 KHz. Surprisingly, the envelope energy did not vary greatly with window, and was relatively independent of load. For the level of damage (Figure 10), it was found that the damage outer race energy was approximately 10x the nominal bearing energy and easily detected (Figure 11).

Similar results were obtained for inner race fault. This data set will be made available at www.mftp.org.

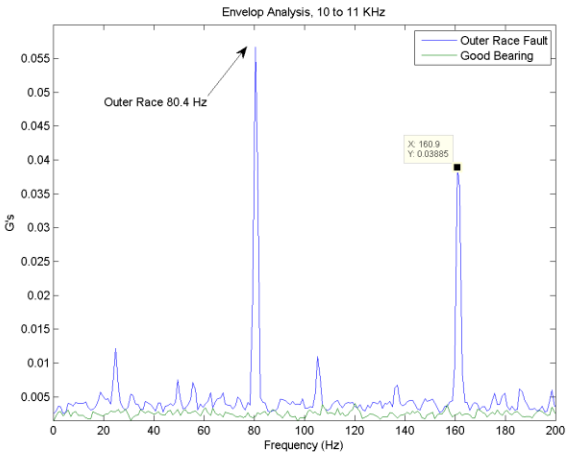

Figure 11 Outer Race Fault Using MEMS Accelerometer

4. Algorithm for the Detection of ICE/Blade Pitch Error

It has been shown that the main rotor is sensitive to both tower shadow and wind shear. These phenomena, due to changes in blade lift as a result of changes in wind speed, could be used to detect difference in lift between each blade. For example, if each blade is identical, then the lift generated on each blade would be identical at a given angle on the hub. This in turn would generate a sinusoidal 3/revolution change in RPM. The amplitude of the Hilbert transform of this 3/rev sinusoid would be nearly constant (McFadden, 1986).

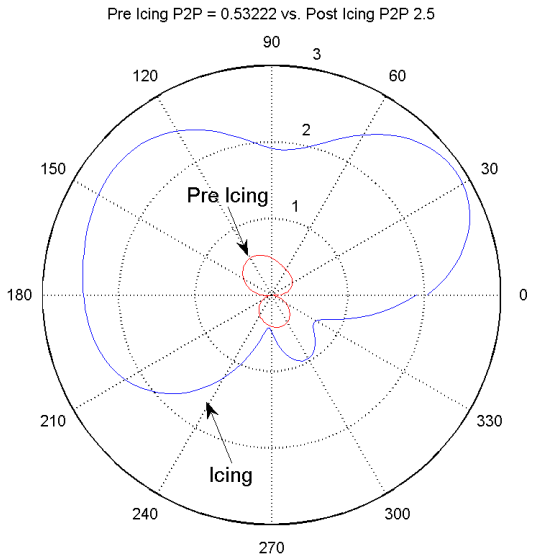

Figure 12 Pre/Post Icing Change in RPM

Consider what would happen if either the blades had icing or if the pitch angle of one blade was in error. The lift generated by that blade would be less. This blade would generate less torque, and as a result, there would a smaller increase in RPM due to when coming out of the tower shadow or as a result of wind shear.

Most operators will not allow one to deliberately fault a turbine. But, as noted (see Figure 2) icing can occur. Since the CMS is down loading raw, time domain data four times a day, if one can capture a raw data collection during an icing event, one can test the proposed hypothesis. This occurred during the January 14 icing even (Figure 12).

During an icing event, the balance of the rotor can be greatly affected. Prior to the icing event, the SO1 imbalance was .001Gs (about .25 ips). The peak-2-peak change in amplitude of the Hilbert transform of the main rotor RPM (AHT) was 0.5 RPM. Just after the icing event, the SO1 acceleration peaked at 0.14Gs (3.5 ips!) with an AHT of 2.5 RPM.

Since blade pitch error is a common cause of underperformance in a wind turbine, this potentially could be a good indicator of that type of fault.

Conclusions

Condition Monitoring of wind turbines poses some unusual requirement on the CMS. The slow shaft rate of the main shaft results in low amplitude, low frequency vibrations, while the high speed side requires high bandwidth to detect gear and bearing faults. This in turn requires the development of highly sensitive accelerometer with a bandwidth from close to DC (0 Hz) to above 10 KHz. While MEMS sensors are typically noisier than PZT accelerometers, it was found that the MEMS sensors were both accurate, an have low enough spectral noise to capture the vibration features on the turbine. This was observed at very low signal intensities and frequencies. This would be difficult to replicate this performance with a PZT accelerometer.

The extremely low frequencies on the main shaft required the development of an in-line decimation enhancement to the TSA. This allowed the sample rate of the sensor to be high enough for bearing envelope analysis, while limiting the length of the TSA to a maximum length of 32768.

The ability of MEMS accelerometers to diagnose and detect stage 3 bearing faults was also validated.

Other peculiarities of a wind turbine are:

- The large change in main rotor RPM due to changing wind conditions over an acquisition, and
- A smaller, 3/revolution change in RPM due to tower shadow and wind shear.

This required the development of an enhanced TSA algorithm to accurately control the 3/rev change in speed.

The ability to detect small changes in main rotor RPM can facilitate icing or blade pitch errors. This was demonstrated during an icing event. This new algorithm will be deployed and verified in the near future.

REFERENCES

ADXL001 product specification, 'http://www.analog.com/en/mems-sensors/mems-accelerometers/adxl001/products/product.html', Analog Devices

Randall, R. (2011) Vibration-based Condition Monitoring: Industrial, Aerospace & Automotive Application, John Wiley, New York.

McFadden, P., (1987). "A revised model for the extraction of periodic waveforms by time domain averaging", Mechanical Systems and Signal Processing 1 (1), pages 83-95.

Bechhoefer, E., Morton, B., (2012). "Condition Monitoring Architecture to Reduce Total Cost of Ownership". *IEEE PHM Conference*, Denver.

Dolan, D., Lehn, R., (2006). "Simulation Model of Wind Turbine 3p Torque Oscillation due to Wind Shear and Tower Shadow", IEEE Transaction on Energy Conversion, VOL. 21, NO. 3.

Bechhoefer, E., Kingsely, M., (2009) "A Review of Time Synchronous Average Algorithms", Annual Conference of the Prognostics and Health Management Society.

McFadden, P.D. (1986). Detecting Fatigue Cracks in Gear by Amplitude and Phase Demodulation of the Meshing Vibration. ASME J. of Vibration, Acoustics, Stress, and Reliability in Design 108, 165-170.

BIOGRAPHIES

Eric Bechhoefer is the chief engineer at NRG Systems. A former naval aviator, Dr. Bechhoefer recently joined NRG from the aerospace industry. Dr. Bechhoefer has 20 patents and over 70 juried papers related to condition monitoring of rotating equipment.

Matthew Wadham-Gagnon is a project manager in wind turbine blade icing related topics at the TechnoCentre Eolien (TCE) since 2011. Prior to joining the TCE, he was involved in the wind energy industry for over 4 years in fields related to structural composite design and composite processing. Matthew has a Master's degree in Mechanical Engineering.

Bruno Boucher is the Operations and Maintenance at the TechnoCentre Eolien (TCE) since 2010. Prior to joining the TCE, he was involved in the wind industry for over 7 years in O&M of wind farm and design of permanent magnet generator. Bruno has a Bachelor's Degree in Electromechanical Systems Engineering.